NUMERICAL SOLUTION OF THE START-UP OF WELL DRILLING FLUID FLOWS

Gabriel Merhy de Oliveira, gabrielm@utfpr.edu.br
Cezar Otaviano Ribeiro Negrão, negrao@utfpr.edu.br
Admilson Teixeira Franco, admilson@utfpr.edu.br
UTFPR - Federal University of Technology - Parana – Av. Sete de Setembro, 3165, CEP 80.230-901 – Curitiba-PR-Brazil

Andre Leibsohn Martins, aleibsohn@petrobras.com.br
Roni Abensur Gandelman, roniag@petrobras.com.br
TEP/CENPES - PETROBRAS S/A – Cidade Universitária, Q.7, Ilha do Fundão, CEP 21.941-915, Rio de Janeiro-RJ

Abstract. *The drilling fluid is designed to build up a gel-like structure, when at rest, in order to avoid cuttings to drop at the bore bottom and therefore to prevent the bit obstruction. As consequence, high pressures, which can be larger than the formation pressure and can damage the well, are needed to break up the gel when circulation resumes. Due to its thixotropic effect, the gel viscosity remains high for a while after the circulation restarts. The gelation may have significant importance, specially, in deep waters where high pressures and low temperatures take place. The current work presents a compressible transient flow model of the start-up flow of drilling fluids, in order to predict borehole pressures. The model comprises one-dimensional conservation equations of mass and momentum and one state equation for the calculation of the fluid density as a function of the pressure. The considered geometry is a concentric annular pipe of length L. Its internal diameter is D_1 and external one, D_2. For a circular pipe, the internal diameter is made equal to zero. The main difference from previous model was the type of boundary condition: Constant flow rate at the pipe inlet rather than the constant pressure. Both Newtonian and non-Newtonian Bingham fluid flows are considered. The governing equations are discretized by the Finite Volume Method using the fully implicit formulation and the first-order upwind scheme. The resulting non-linear algebraic equations are iteratively solved. The model results were corroborated with an analytical solution for Newtonian flows. Case studies are conducted to evaluate the effect of fluid flow properties, well geometry and flow rate on borehole pressures. For Bingham fluid flow one can observe that large pressures (compared with Newtonian fluid flow) are observed when constant flow rate are input as boundary condition. Pressure peaks caused by the acoustic wave propagation can be more intense in low compressible fluid flow, low viscosity fluid and in smaller length pipes. The model can be applied to predict the time-dependent pressure field and pressure peaks during the restart of drilling fluid operations.*

Keywords*: start-up flow, drilling fluid, Bingham fluid, compressible flow, transient flow*

1. INTRODUCTION

In oil well drilling, a fluid is pumped through a drill pipe. The fluid flows to the bottom of the hole and returns by the annular space between the drill pipe and the well wall, carrying the cuttings formed while drilling. During drilling stoppages, the fluid gellifies in order to avoid cuttings to fall down in the annular space obstructing the bit. The flow restart requires higher than the usual operational pressures to break the gel down. High pressure peaks may damage the well structure. Therefore, the study of the wave pressure propagation during the flow restart is essential to predict the pressure peaks.

The mathematical modeling can be quite useful to understand the phenomenon and to predict pressure peaks during the flow restart of a gellified material. Although some works were dedicated to study the problem most of them were applied to the start-up of waxy crude oils at low temperature. For instance, Sestak *et al.* (1987), Cawkwell and Charles (1987), Chang *et al.* (1999) and Davidson *et al.* (2004) considered that the waxy crude oil filled completely the pipe and them it is displaced by a non-gellified oil. Chang´s *et al.* (1999) e Sestak´s *et al.* (1987) works disregarded the inertial effects in the momentum equation and shear forces are based on the fully developed flow. The time variation of flow occurs only due to the time-change of the rheology properties. Davidson *et al.* (2004) included the compressibility effect in the Chang´s *et al.* (1999) model but did not considered the inertia terms in the momentum conservation equation. Although Cawkwell and Charles (1987) have disregarded the advective terms in the momentum conservation equation they considered the fluid flow as transient and compressible. Vinay *et al.* (2006) presented a 2D transient model to simulate the start-up of a Bingham fluid. In a second work, Vinay *et al.* (2007) developed a 1D model and compared the results to their 2D model with good agreement. Nevertheless, Vinay *et al.* (2007) showed the solution of the one-dimensional model is much faster their 1D counterpart. In order to reduce the computational time, the same authors (Wachs *et al.*, 2009) developed a 1.5D model in which they merged the 2D and the 1D model. Besides, they evaluated the compressibility and thixotropy in the fluid flow restart.

The current work presents a mathematical model for the start-up of drilling fluids in horizontal pipes. The transient flow is considered isothermal, one-dimensional and compressible. Differently from the above works, both the transient

and advective terms are included in the equations. Besides, the friction factor concept for fully developed flows for both Newtonian and Bingham fluid is applied to the computation of viscous effects. The governing equations are discretized by the Finite Volume Method with the fully implicit and first-order upwind schemes. The set of discretized equations are solved iteratively.

2. MATHEMATICAL MODEL

2.1 System Geometry and Hypothesis

Although the drilling fluid flows through the drill pipe and the annular space (see Fig. 1a), the geometry is simplified to a horizontal annular space. The length, internal and external diameters are, respectively, L, D_1 and D_2, as shown in Fig. 1b. To simulate a pipeline flow, the internal diameter can be taken as zero.
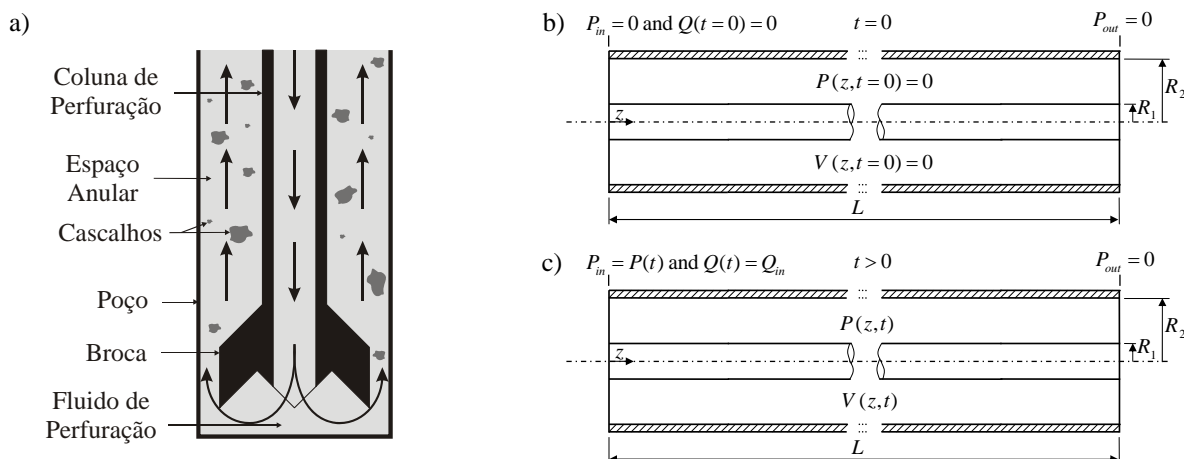
Figure 1. (a) Scheme of the wellbore, drill pipe and drill bit. Problem domain at: (b) $t = 0$ and (c) $t > 0$.

2.2 Governing Equations

Considering the fluid flow as one-dimensional, as shown in Fig. 1, the governing equations of mass and momentum can be written, respectively, as:

$$\frac{\partial \rho}{\partial t} + \frac{\partial (\rho V)}{\partial z} = 0 \tag{1}$$

$$\frac{\partial (\rho V)}{\partial t} + \frac{\partial (\rho V V)}{\partial z} = -\frac{\partial P}{\partial z} - \frac{2 f \rho V^2}{D_h} \tag{2}$$

where ρ, V and P are the average values of density, velocity and pressure in the cross sectional area, respectively, f is the Fanning friction factor, which is evaluated according to the fluid flow, fluid properties and geometry (pipe or annular). t is the time and z is the axial position. D_h is the hydraulic diameter, which is defined as $D_2 - D_1$ for the annular space and as D_2 for the pipe ($D_1 = 0$).

Once the flow is compressible, density is function of pressure and the flow is isothermal. Besides, the pipe is considered completely rigid. By definition, the fluid compressibility, α, can be written as (Anderson, 1990):

$$\alpha = \frac{1}{\rho} \frac{\partial \rho}{\partial P} \bigg|_T \tag{3}$$

Assuming the compressibility is constant for the pressure range analyzed, Eq. (3) can be rearranged and integrated from a reference state to any other:

$$P = P_0 + \frac{1}{\alpha} \ln \left(\frac{\rho}{\rho_0} \right) \tag{4}$$

where ρ_0 and P_0 are, respectively, the density and pressure for the reference state. According to Anderson (1990), the fluid compressibility, the density and the pressure wave speed are correlated by the equation:

$$\alpha = \frac{1}{\rho_0 a^2} \tag{5}$$

where a is the pressure wave speed for an inelastic pipe.

2.3 Constitutive Equation and Friction Factor

The drilling fluid is considered to be a Bingham plastic:

$$\tau = \tau_0 + \eta\dot{\gamma} \tag{6}$$

where τ is the shear stress, $\dot{\gamma}$ is the shear strain rate, τ_0 is the yield stress and η is the fluid plastic viscosity. This constitutive equation is implicitly taken into account in the calculation of the friction factor.

The friction factor depends on the kind of fluid, its properties and flow geometry. In the current work, the flow is assumed laminar. For the non-Newtonian Bingham flow in a circular pipe, the Fanning friction factor is employed (Chang *et al.*, 1999):

$$f_T = \frac{16}{\mathrm{Re}_{z,t}}\left(1 + \frac{\mathrm{He}_{z,t}}{6\,\mathrm{Re}_{z,t}} - \frac{\mathrm{He}_{z,t}^4}{3 f_T^{\,3}\,\mathrm{Re}_{z,t}^7}\right) \tag{7}$$

where $\mathrm{Re}_{z,t} = \rho V D_h / \eta$ is the Reynolds number and $\mathrm{He}_{z,t} = \rho \tau_0 D_h^{\,2} / \eta^2$ is the Hedstrom number. The subscript T means the friction factor is computed for a circular pipe. The t and z subscripts of the Reynolds and Hedstrom numbers means they are vary with time and the axial position, respectively. Eq. (7) is reduced to the Newtonian friction factor as the Hedstrom number (or the yield stress) approaches zero.

The following Fanning friction factor is adopted to the annular pipe (Fontenot and Clark, 1974):

$$f_A = \frac{24}{\gamma\,\mathrm{Re}_{z,t}} \quad \mathrm{e} \quad \gamma = 1 - \frac{\gamma\mathrm{He}_{z,t}}{8\,\mathrm{Re}_{z,t}} + \frac{1}{2}\left(\frac{\gamma\mathrm{He}_{z,t}}{12\,\mathrm{Re}_{z,t}}\right)^3 \tag{8}$$

where the index A means annular space and γ is the conductance of the Bingham fluid.

For a zero yield stress, $\gamma = 1$, and Eq. (8) is reduced to the laminar flow friction factor of a Newtonian fluid in a annular space. According to Fontenot and Clark (1974), the fluid flow can be considered to be laminar if $\gamma\,\mathrm{Re}_{z,t} \le 2000$.

2.4 Dimensionless Governing Equations

The axial position, the time and density are normalized according to the following:

$$\bar{z} = \frac{z}{L}, \quad \bar{t} = t\frac{a}{L} \quad \text{and} \quad \bar{\rho} = \frac{\rho}{\rho_0} \tag{9}$$

The dimensionless velocity is defined as a function of the pipe inlet velocity (V_{in}) and the pressure as a function of the pressure gradient (ΔP_{in}) of a Newtonian steady-state flow:

$$\bar{V}(\bar{z},\bar{t}) = \frac{V(z,t)}{V_{in}}, \qquad \bar{P}(\bar{z},\bar{t}) = \frac{P(z,t)}{\Delta P_{in}} \qquad \text{and} \qquad \Delta P_{in} = \frac{32\zeta\eta L V_{in}}{D_h^2} \tag{10}$$

ζ is a geometric parameter of the annular space which is defined as:

$$\zeta = \frac{(D_2 - D_1)^2}{D_2^2 + D_1^2 - \dfrac{(D_2^2 - D_1^2)}{\ln(D_2/D_1)}} \tag{11}$$

For a circular pipe, ζ is equal to 1.0, and for a narrow annular space ($D_1/D_2 \ge 0.5$), its value is approximately 1.5. In the current work, all annular spaces are considered narrow.

By employing the dimensionless variables of Eqs. (9) and (10), Eqs. (1) to (3) can be re-written as:

$$\left(\frac{1}{\alpha^*}\right)^{1/2}\left(\frac{32\zeta}{\text{Re}\,\delta}\right)^{1/2}\frac{\partial\bar{\rho}}{\partial\bar{t}}+\frac{\partial(\bar{\rho}\bar{V})}{\partial\bar{z}}=0 \tag{12}$$

$$\left(\frac{1}{\alpha^*}\right)^{1/2}\left(\frac{32\zeta}{\text{Re}\,\delta}\right)^{1/2}\frac{\partial(\bar{\rho}\bar{V})}{\partial\bar{t}}+\frac{\partial(\bar{\rho}\bar{V}\bar{V})}{\partial\bar{z}}=-\left(\frac{32\zeta}{\text{Re}\,\delta}\right)\frac{\partial\bar{P}}{\partial\bar{z}}-\frac{2f\,\bar{\rho}\bar{V}^2}{\delta} \tag{13}$$

$$\frac{d\bar{\rho}}{d\bar{P}}=\alpha^*\bar{\rho} \tag{14}$$

where Re (the Reynolds number), α^* (the dimensionless compressibility), δ (the aspect ratio) and the Bingham number are the characteristic parameters of the problem:

$$\text{Re}=\frac{\rho_o V_{in} D_h}{\eta},\quad \alpha^*=\alpha P_{in}=\left(\frac{32\zeta}{\text{Re}\,\delta}\right)\left(\frac{V_{in}}{a}\right)^2,\quad \delta=\frac{D_h}{L}\quad\text{and}\quad B=\frac{\tau_0 D_h}{8\zeta\eta V_{in}} \tag{15}$$

2.5 Initial and Boundary Conditions

As an initial condition, the drilling fluid is admitted to rest within the pipe and therefore, the velocity field is null ($\bar{V}(\bar{z},\bar{t}=0)=0$). Initially, the fluid density is uniform within the whole ($\bar{\rho}=1$). Therefore, according to Eq. (14), the initial pressure filed is also uniform and equal to zero $\bar{P}(\bar{z},\bar{t}=0)=0$.

To restart the fluid flow of the gellified fluid, a pump pressurizes another fluid to the pipe. Therefore, the gellified fluid starts to be displaced. It is assumed that the pump provides a constant volumetric flow at the pipe inlet or a constant average velocity ($\bar{V}(\bar{z}=0,\bar{t})=1$). At the pipe outlet, the density is assumed and consequently, the pressure, as constant ($\bar{\rho}(\bar{z}=1,\bar{t})=1$ and $\bar{P}(\bar{z}=1,\bar{t})=0$).

3. SOLUTION OF THE EQUATIONS

3.1 Discretization of the Equations

The governing equations of the problem are discretized by employing the Finite Volume Method, as proposed by Patankar (1980). The pressure and velocity grids are staggered, as the pressure is evaluated at the finite volume faces and the velocity at the center of the volumes. Fig. 2 shows a grid scheme for an annular space domain. The domain is divided into N finite volumes of length $\Delta\bar{z}$. In Fig. 2, the pressure position is indicated by a small i and the velocity position by a capital I. With this grid, i ranges from 1 to $N+1$ and I, from 1 to N. Note that these are average values of the variables across the sectional area. The fully implicit and the first order up-wind schemes are employed as interpolation functions in time and space respectively.
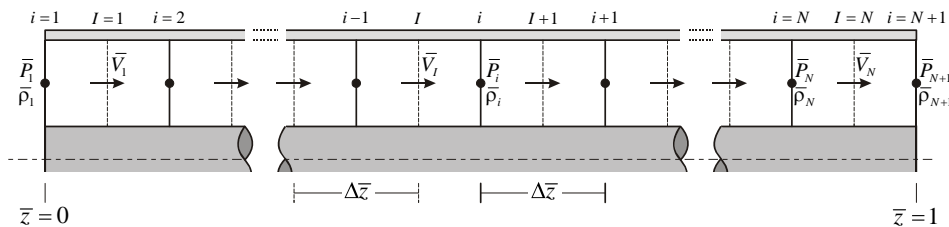
Figure 2. View of the employed grid.

3.2 Solution Method

The non-linear discretized equations are solved iteratively at each time-step. The whole pipe is divided into N finite volumes of length $\Delta\bar{z}$, as shown in Fig. 2. In the current work, a 500 volume grid is employed. Initially, the pressure and velocity fields are estimated and the governing equations are solved iteratively until convergence. After convergence, the solution evolves to the next time-step and the computation is repeated. This time evolution takes places until the steady-state is reached.

As the fluid flow is transient and compressible, the equations are hyperbolic. To avoid instabilities and numerical errors, the literature (Wylie *et al.*, 1993, Fortuna, 2000) suggests that the time and space grids be related by the pressure wave speed according to:

$$CFL = \frac{\Delta \bar{t}}{\Delta \bar{z}}$$ (16)

Independently to discretization scheme used (implicit or explicit), a good practice to reduce numerical diffusion and/or dispersion is to keep $CFL \approx 1.0$ (Ferziger and Peric, 1996). As the pressure and velocity grids are a half volume staggered, the best results were observed for $CFL \approx 0.5$. Therefore, $CFL = 0.5$ is employed for all cases shown below.

4. RESULTS AND DISCUSSION

4.1 Model Validation

In order to validate the model, the results of an analytical solution are compared with the current model results. As Eqs. (12), (13) and (14) do not have a known analytical solution, they are simplified for low compressible flow case. The hypothesis are: i) the non-linear advective terms, $\bar{V} \partial \bar{\rho} / \partial \bar{z}$ e $\bar{\rho} \bar{V} \partial \bar{V} / \partial \bar{z}$, are disregarded in mass and momentum conservation equations, respectively; ii) the density is substituted into the mass conservation equation by employing the equation of state (Eq. (14)); iii) the mass conservation equation is substituted into the momentum conservation equation (Eq. (13)) and iv) the fluid is considered Newtonian ($\tau_0 = 0$ or $B = 0$). The mass and momentum conservation equations are derived in respect to $\bar{z}$ and $\bar{t}$, respectively, and they are subtracted from each other:

$$\bar{\rho} \frac{\partial^2 \bar{V}}{\partial \bar{t}^2} = \frac{\partial^2 V}{\partial z^2} - \lambda \frac{\partial \bar{V}}{\partial \bar{t}}$$ (17)

where λ is a constant that represents the viscous effect ($\lambda^2 = 32\zeta\alpha^* / \mathrm{Re}\,\delta$). This second-order linear equation depends only on the velocity and equivalent equation can be obtained for pressure:

$$\bar{\rho} \frac{\partial^2 \bar{P}}{\partial \bar{t}^2} = a^2 \frac{\partial^2 \bar{P}}{\partial \bar{z}^2} - \lambda \frac{\partial \bar{P}}{\partial \bar{t}}$$ (18)

For the constant flow rate boundary condition at the pipe inlet, the solution of equations Eqs. (17) and (18) can be written as:

$$\bar{V}\left(\bar{z},\bar{t}\right) = \left\{ 1 - 2e^{\frac{-\lambda\bar{t}}{2}} \sum_{j=1}^{\infty} \left[\frac{1}{\beta_j} \sin\beta_j\bar{z} \left(\cos\omega_j\bar{t} + \frac{\lambda}{2\omega_j}\sin\omega_j\bar{t} \right) \right] \right\}$$ (19)

$$\bar{P}\left(\bar{z},\bar{t}\right) = \left(1 - \bar{z}\right) + \frac{2e^{\frac{-\lambda t}{2}}}{\lambda} \sum_{j=1}^{\infty} \left\{ \frac{1}{\beta_j{}^2} \cos\beta_j\bar{z} \left[\left(\omega_j - \frac{\lambda^2}{4\omega_j} \right) \sin\omega_j\bar{t} - \lambda\cos\omega_j\bar{t} \right] \right\}$$ (20)

where $\beta_j = \left(j - 1/2\right)\pi$ and $\omega_j^2 = \beta_j^2 - \lambda^2 / 4$.

For an annular pipe with $\mathrm{Re} = 500$, $\alpha^* = 0.001$, $B = 0$, $\delta = 0.0001$ and $\zeta = 1.5$, λ is equal to 0.98. Figs. 3 and 4 compare the current model and analytical solution results. Fig. 3 presents the time change of pressure in three positions along the pipe; at the inlet ($\bar{z} = 0$), at the middle ($\bar{z} = 0.5$) and near pipe outlet ($\bar{z} = 0.9$) and Fig. 4 shows the velocity change at $\bar{z} = 0.1$, $\bar{z} = 0.5$ and at the pipe outlet ($\bar{z} = 1$). As already said, a 500 finite volume grid was employed in the comparison. As can be seen, the results are quite close. Grid refining can approximate the results even more. However, the computational time increases exponentially. Therefore, the 500 grid volumes are used for all simulation shown below.

One can see that both pressure and velocity show oscillation with time. These oscillations are due to pressure propagation that reflects in both pipe ends. The pressure behavior in Fig. 3 can be understood by analyzing the pressure change with the axial position in several time instants (see Fig. 5). In Fig. 5a are shown the pressure field at five dimensionless times (0.002, 0.25, 0.5, 0.75 and 1.0). Note that before $\bar{t} = 1.0$ the pressure wave did not propagate through the whole pipe. For $\bar{t} = 0.5$, the pressure wave traveled through half the pipe length. In other words, pump pressure is only felt on half of the pipe and the other half is kept at zero pressure.
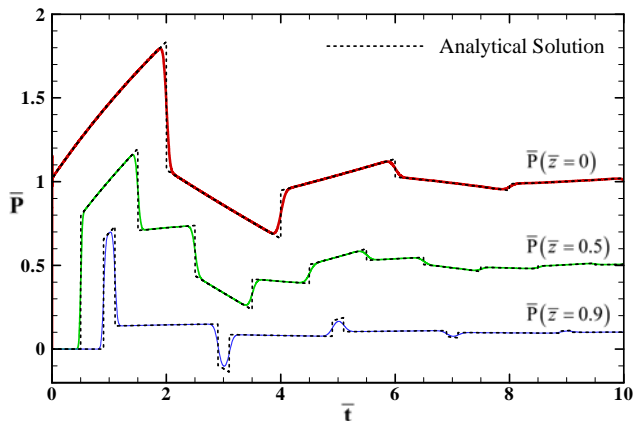
Figure 3. Time change of pressure. $\text{Re} = 500$, $\alpha^* = 0.001$, $B = 0$, $\delta = 0.0001$ e $\zeta = 1.5$.
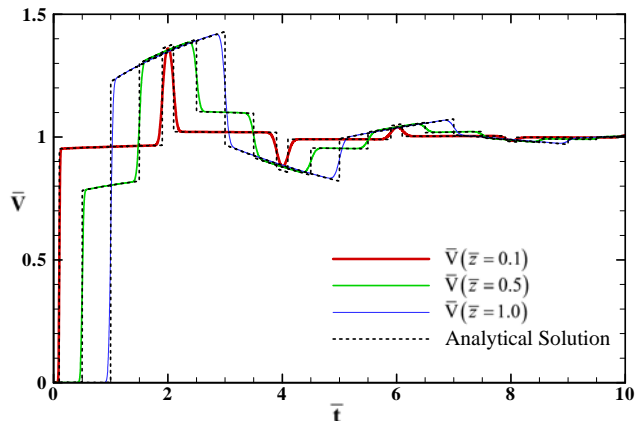
Figure 4. Time change of velocity. $\text{Re} = 500$, $\alpha^* = 0.001$, $B = 0$, $\delta = 0.0001$ e $\zeta = 1.5$.

In Fig. 5b are shown the pressure profiles between time $\bar{t} = 1.0$ and $\bar{t} = 3.0$. At the pipe end and time $\bar{t} = 1.0$, the pressure wave reflects and starts to propagates on reverse direction; from the pipe outlet to the inlet. The propagation on this direction takes place until $\bar{t} = 2.0$, as the pressure reaches the inlet and reflects again. The reflection occurs continuously before being completely dissipation by the viscous force. Fig. 5c illustrates the pressure dissipation between 3.0 and 4.0 and also the pressure filed for $\bar{t} = 20.0$, which is almost the steady-state. In the steady-state, the pressure changes linearly with the pipe length.
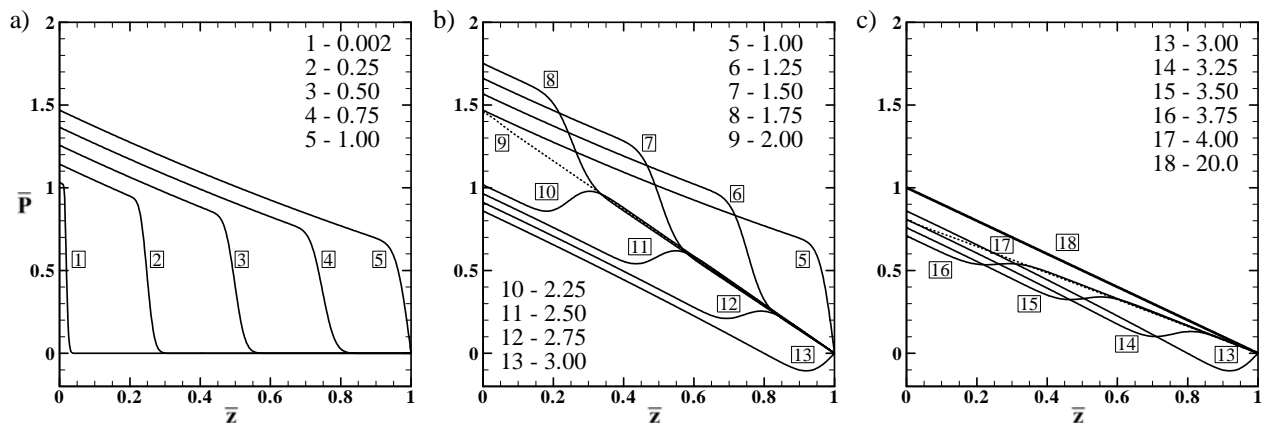
Figure 5. Pressure change with pipe length for several dimensionless times. $\text{Re} = 500$, $\alpha^* = 0,001$, $B = 0$, $\delta = 0,0001$ and $\zeta = 1,5$.

One can see in Fig. 3 that the inlet pressure rises continuously to its maximum value ($\bar{P} = 1.82$) at approximately $\bar{t} = 2.0$. At this time, the pressure wave reflects at the inlet and the pressure falls down immediately. The pressure then continues to decrease as the pressure wave propagates back to the outlet and forward to the inlet, when the pressure jumps again at $\bar{t} = 4.0$. This cycle takes place until the pressure wave is completely dissipated and the inlet pressure stabilizes at 1.0. For $\bar{z} = 0.9$, the pressure peak length is shorter than its inlet counterpart. Nevertheless, the its first peak is 7.3 times higher than the steady-state value ($\bar{P}_{RP}(\bar{z} = 0) = 0.1$). Fig. 4 shows that the fluid flow in any position starts when the pressure wave reaches such position. Besides, the wave reflection alters significantly the fluid velocity, as the outlet velocity is about 1.4 times higher than the inlet value at time $\bar{t} = 3.0$.

4.2 Sensitivity Analysis

This section presents the influence of the main parameters in the fluid flow, namely, Reynolds number, dimensionless compressibility and Bingham number.

4.2.1 The Effect of the Reynolds Number

The influence of the Reynolds number in the time change of inlet pressure ($\overline{z} = 0$) can be seen in Fig. 6. As the inertial effects decreases in comparison to the viscous effect (reduction of Re), the pressure wave undergoes a larger dissipation. The dissipation is related to the necessary time to reach the steady-state; the smaller the Reynolds number the larger the time to reach the steady-state. However, for higher Reynolds number, the pressure wave has enough energy to reflect several times before being completely dissipated, increasing the time to reach the steady-state. Although Fig. 6 do not show the steady-state for $Re = 1$, the steady-state is Reynolds number independent ($\overline{P}_{RP}\left(\overline{z} = 0\right) = 2.41$). The steady-state pressure is higher than 1.0 because the fluid is a Bingham plastic ($B = 1.0$). In section 3.2.3, this result is better explained.

Fig. 7 shows the velocity changes with time for three different positions, $\overline{z} = 0.1$, $\overline{z} = 0.5$ and $\overline{z} = 1$, and $Re = 100$. The outlet velocity starts to change only at $\overline{t} = 1.82$ because of pressure wave dissipation. The velocity $\overline{z} = 0.5$ changes its time evolution at $\overline{t} = 2.32$. This faster increase of velocity takes place after the pressure wave going forward and back to the middle of the pipe. This effect also accelerates the fluid at $\overline{z} = 0.1$, as shown in Fig. 7.
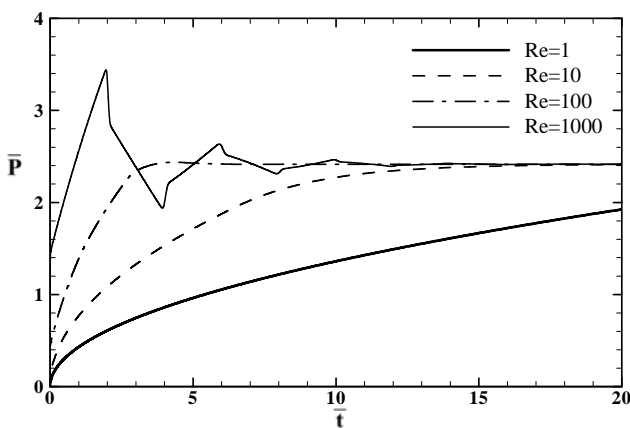
Figure 6. Effect of Reynolds number on the time change of pressure at $\overline{z} = 0$. $\alpha^* = 0.001$, $B = 1.0$, $\delta = 0.0001$ and $\zeta = 1.5$.
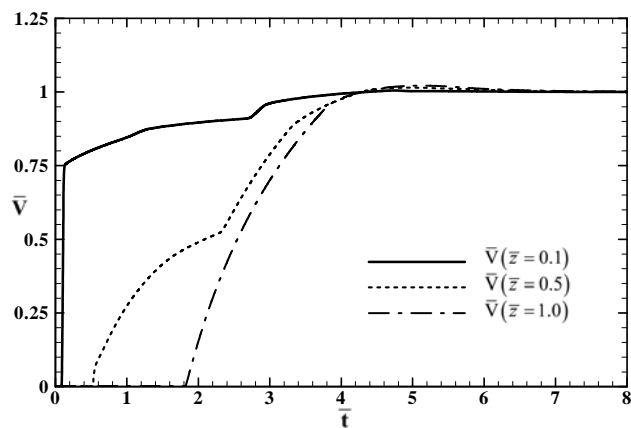
Figure 7. Time change of $\overline{V}$ at $\overline{z} = 0.1$, $\overline{z} = 0.5$ and $\overline{z} = 1$. $Re = 100$, $\alpha^* = 0.001$, $B = 1.0$, $\delta = 0.0001$ and $\zeta = 1.5$.

4.2.2 The Effect of the Dimensionless Compressibility

Fig. 8 shows the inlet pressure change as a function of the dimensionless compressibility. One can see the pressure wave dissipation increases with the dimensionless compressibility. Pressure peaks are only observed for smaller compressibility. Besides, to keep the same flow rate for a higher compressible fluid, a higher inlet pressure is necessary. For $\alpha^* = 0.001$, the inlet steady-state pressure is 2.42, and for $\alpha^* = 0.1$, this value is approximately 6.0 higher ($\overline{P}_{RP}\left(\overline{z} = 0\right) = 2.56$).

Despite the different Reynolds numbers, the curve for $\alpha^* = 0.001$ of Fig. 8 and that for $Re = 1000$ of Fig. 6 are identical. The analysis of Eqs. (12) and (13) shows the dimensionless governing parameters of the flow are: α^*, $32\zeta/Re\,\delta$ and B. Therefore, the results coincide because all three parameters of these two cases are the same. One can conclude that the effect of increasing of the aspect ratio is equivalent to the increase of the Reynolds number.

Fig. 9 shows that the pressure wave reaches the pipe outlet at the expected time ($\overline{t} = 1.0$) for the less compressible case and for the highest compressibility, this time increases to about $\overline{t} = 5.2$. This delay is related to the pressure wave dissipation as the compressibility increases. Besides, the steady-state average velocity at the pipe outlet, as the inlet pressure, increases with the fluid compressibility. The difference between the imposed inlet velocity, $\overline{V}(\overline{z} = 0, t) = 1.0$, and the steady-state outlet velocity is due to the conservation of mass. The high pressure at the pipe inlet makes the inlet density smaller than the outlet counterpart. In order to keep the same mass flow rate, the average outlet velocity must be higher than the inlet one. For the most compressible case, the outlet velocity is about 1.27 times higher than the inlet one ($\overline{V}_{RP}(\overline{z} = 1) = 1.27$).
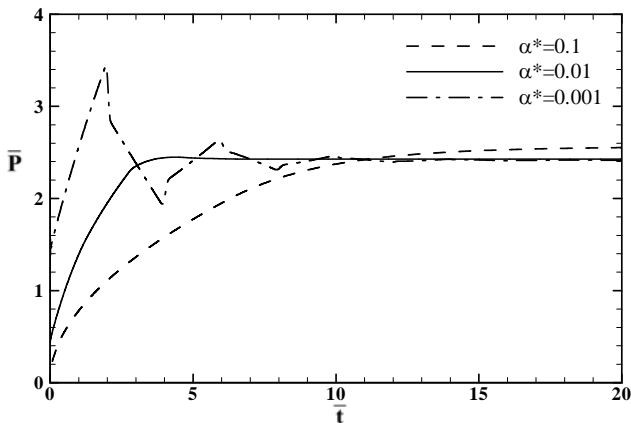
Figure 8. Effect of α^* in the time change of $\overline{P}$ at $\overline{z} = 0$. $\mathrm{Re} = 100$, $\mathrm{B} = 1.0$, $\delta = 0.001$ and $\zeta = 1.5$.
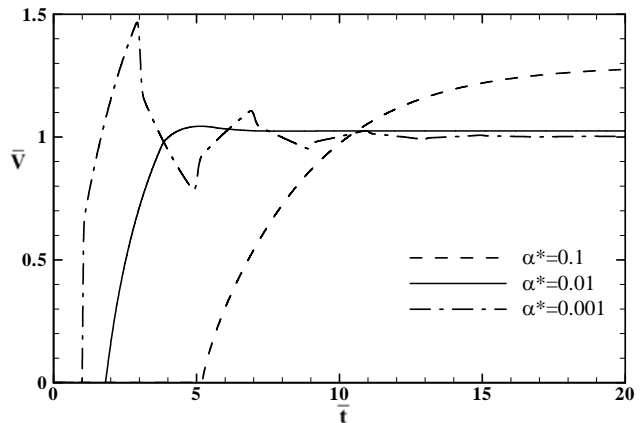
Figure 9. Effect of α^* in the time change of $\overline{V}$ at $\overline{z} = 1$. $\mathrm{Re} = 100$, $\mathrm{B} = 1.0$, $\delta = 0.001$ and $\zeta = 1.5$.

4.2.3 The Effect of the Bingham Number

The Bingham number is directly related to the yield stress of the fluid. A fluid with a high yield stress requires a high pressure to start-up. The effect of the Bingham number on the flow start-up is now analyzed. Fig. 10 shows that the steady-state pressure for a low compressibility, Newtonian ($\mathrm{B} = 0$) fluid stabilizes at 1.0. To provide the same flow rate, the steady-state pressure increases with the Bingham number. For $\mathrm{B}=5.0$, the inlet steady-state pressure is 7.3 larger than the Newtonian fluid pressure. As shown in Fig. 11, the pressure oscillation are reduced with the increase of the Bingham number. In comparison with other Bingham numbers, the pressure wave takes a longer time to reach the pipe end for $\mathrm{B} = 5.0$. Besides, the pressure peak at $\overline{z} = 0.9$ is relatively small in comparison to the steady state pressure.
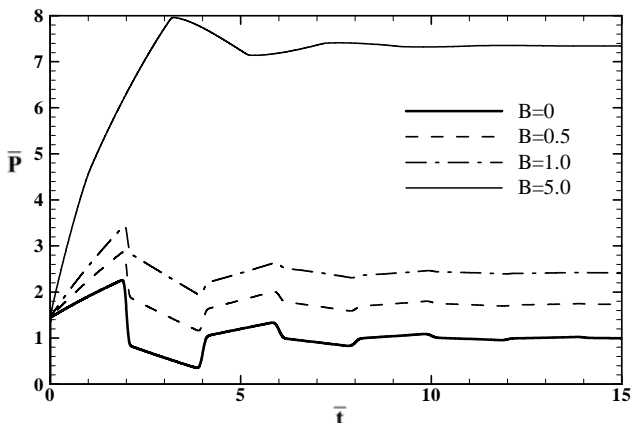
Figure 10. Effect of B in the time variation of $\overline{P}$ at $\overline{z} = 0$. $\mathrm{Re} = 100$, $\alpha^* = 0.001$, $\delta = 0.001$ and $\zeta = 1.5$.
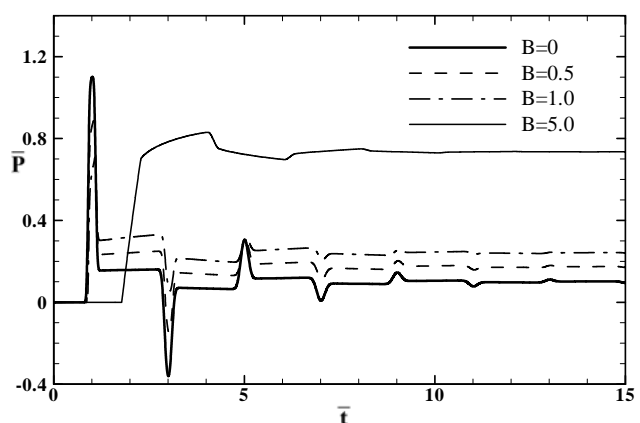
Figure 11. Effect of B in the time variation of $\overline{P}$ at $\overline{z} = 0.9$. $\mathrm{Re} = 100$, $\alpha^* = 0.001$, $\delta = 0.001$ and $\zeta = 1.5$.

5. CONCLUSIONS

This work presents a mathematical model to simulate the flow start-up of drilling fluids. The viscous effect is taken into account by employing the friction factor concept. The governing equations (conservation of mass, momentum and the equation of state) are normalized and discretized by the Finite Volume Method, implicit and up-wind scheme. The system of non-linear algebraic equations is solved iteratively at each time-step.

The numerical results are compared to analytical solution results for Newtonian fluids and a good agreement is obtained.

A sensitivity analysis of Reynolds and Bingham numbers, dimensionless compressibility and aspect ratio is conducted and the conclusions are:

i) The smaller the Reynolds number the higher the pressure wave dissipation and consequently, the smaller the pressure peaks. The reason for that is the increase of the viscous effect in comparison to the inertia effects;

ii) Low compressibility fluids present more oscillations. As the compressibility increases the oscillations reduce or even disappear;

iii) The aspect ratio is provides the same effect as the Reynolds number. In other words, for a large pipe length in comparison the diameter (small aspect ratio), there is a large region to dissipate the pressure energy, contributing to a smooth pressure propagation. The opposite is also true for a large aspect ratio.

iv) The higher the Bingham number the larger pressure magnitude and the smaller the pressure oscillation. The reason is the larger apparent viscosity as the Bingham number increases.

6. ACKNOWLEDGEMENTS

7. REFERENCES

Anderson, J.D.,1990, "Modern Compressible Flow", Ed. McGraw-Hill, N. York, U. States, 650 p.

Cawkwell, M.G. and Charles, M.E.,1987, "An Improved Model for Start-up of Pipelines Containing Gelled Crude Oil", J. of Pipelines, Vol. 7, pp. 41-52.

Chang, C., Rønningsen, H.P. and Nguyen, Q.D.,1999, "Isothermal Start-up of Pipeline Transporting Waxy Crude Oil", J. of Non-Newtonian F. Mechanics, Vol. 87, pp. 127-154.

Davidson, M.R., Nguyen, Q.D., Chang,C. and Ronningsten, H.P.,2004, "A Model for Restart of a Pipeline with Compressible Gelled Waxy Crude Oil", J. of Non-Newtonian F. Mechanics, Vol. 123, No. 2-3, pp. 269-280.

Ferziger, J.H. and Peric, M., 1996, "Computational Methods for Fluid Dynamics", Ed. Springer-Verlag, Berlin, German, 364 p.

Fontenot, J.E. and Clark, R.K.,1974, "An Improved Method for Calculating Swab and Surge Pressures and Circulating Pressures in a Drilling Well", Soc. of Petroleum Eng. J. (SPE 4521), Vol. 14, No 5, pp 451-462.

Fortuna, A. O, 2000, "Técnicas Computacionais para Dinâmica dos Fluidos. Conceitos Básicos e Aplicações", Ed. da Universidade de São Paulo, S. Paulo, Brazil, 426 p.

Patankar, S.V., 1980, "Numerical Heat Transfer and Fluid Flow", Ed. Taylor & Francis, Washington, U. States, 197 p.

Sestak, J., Cawkwell, M.G., Charles, M.E. and Houskas, M.,1987, "Start-up of Gelled Crude Oil Pipelines", J. of Pipelines, Vol. 6, pp. 15-24.

Vinay, G., Wachs, A. and Agassant, J.F.,2006, "Numerical Simulation of Weakly Compressible Bingham Flows: The Restart of Pipeline Flows of Waxy Crude Oils", J. of Non-Newtonian F. Mechanics, Vol. 136, No. 2-3, pp. 93-105.

Vinay, G., Wachs, A. and Frigaard, I., 2007, "Start-up Transients and Efficient Computation of Isothermal Waxy Crude Oil Flows", J. of Non-Newtonian Fluid Mechanics, Vol. 143, No 2-3, pp. 141-156.

Wachs, A., Vinay, G., and Frigaard, I. 2009, "A 1.5D Numerical Model for the Start Up of Weakly Compressible Flow of a Viscoplastic and Thixotropic Fluid in Pipelines". J. of Non-Newtonian F. Mechanics,Vol. 159, pp. 81-94.

Wylie, E. B., Streeter, V. L., and Suo, L., 1993, "Fluid Transients in Systems", Ed. P. Hall, N. Jersey, U. States, 463 p.

8. RESPONSIBILITY NOTICE

The authors are the only responsible for the printed material included in this paper.